Deltaic Burial of Authigenic Calcite Modulates the Carbon Balance of Hardwater Lakes

Benedict V. A. Mittelbach^{1,2}, Margot E. White^{1,3}, Timo M. Y. Rhyner¹, Negar Haghipour^{1,4}, Marie-Elodie Perga⁵, Nathalie Dubois^{1,2}, Timothy I. Eglinton¹

15 Correspondence to: Benedict V. A. Mittelbach (bmittelbach@ethz.ch)

Abstract. Inland waters play an important role in the terrestrial carbon cycle by burying carbon in aquatic sediments while simultaneously releasing CO₂ to the atmosphere and laterally exporting carbon along the land-ocean aquatic continuum. Especially in hardwater lakes, the close connection between primary production and calcite precipitation results in a poorly understood balance of carbon burial and release, with stronger coupling of organic and inorganic processes than in softwater lakes. To better understand these dynamics, we analyzed organic and inorganic carbon fluxes in a yearlong (June 2022 to June 2023) sediment trap study in Lake Geneva, the largest natural lake in Western Europe. Two sediment traps - one deployed in the subaqueous delta of the upper Rhône River, the other in the lake's deepest basin - were sampled monthly. Analyzing radiocarbon (¹⁴C) signatures of particulate organic and inorganic carbon allowed us to resolve allochthonous (external) and autochthonous (internal) contributions to absolute carbon fluxes. We found that the flux of autochthonous particulate inorganic carbon in the river-proximal deltaic site was approximately four times higher than in the distal one. This is likely the result of calcite precipitation driven by increased fluvial supply of nutrients and suspended carbonate-bearing particles. Sediment core analysis in the same location suggests efficient preservation of this calcite over centennial timescales, which we conservatively estimate around 7-10 Gg C yr⁻¹ lake-wide. This indicates at least partial offset of the CO₂ released during calcite precipitation and is an important flux to be considered in mechanistic carbon cycle models.

1 Introduction

Inland waters are key sites for integrating, processing, and storing carbon (C), thus representing a key component of the terrestrial C cycle. The long residence time of water in lakes and reservoirs makes them important sites for the processing of C, leading to its burial or outgassing (Cole et al., 2007; Tranvik et al., 2018). The burial of particulate organic carbon (POC)

¹Department of Earth and Planetary Sciences, ETH Zurich, Zurich, Switzerland

²Department of Surface Waters Research and Management, Eawag, Dübendorf, Switzerland

³Department of Earth, Ocean and Atmospheric Sciences, University of British Columbia, Vancouver, Canada,

^{10 &}lt;sup>4</sup>Laboratory for Ion Beam Physics, Department of Physics, ETH Zurich, Zurich, Switzerland

⁵Faculty of Geosciences and Environment, Institute of Earth Surface Dynamics, University of Lausanne, Lausanne, Switzerland

or particulate inorganic carbon (PIC) in lake sediments can act as a sink of C. However, at the same time, outgassing of CO₂ from the dissolved inorganic carbon (DIC) pool to the atmosphere, e.g., from the remineralization of organic carbon (OC), represents a source of CO₂. The balance between burial and outgassing processes varies both spatially and seasonally. Further, implications for regional and global C budgets critically depend on the source and type of processed C.

Large lakes, in particular, capture significant amounts of organic and inorganic C from various sources in their catchments (allochthonous C) and from in-lake processes such as aquatic primary productivity (autochthonous C), with differing climatic implications. Allochthonous POC (POC_{Allo}) can consist of fast-cycling C such as biospheric POC, which rapidly incorporates atmospheric CO₂, or from soils, where it can be stored on up to millennial timescales, acting more subtly on present-day climate (Eglinton et al., 2021). The erosion and re-burial of POC stored in bedrock on even longer, geological timescales, termed petrogenic POC, does not influence present-day CO₂ levels. Similarly, allochthonous PIC (PIC_{Allo}) contains eroded fragments of carbonate rocks, which formed millions of years ago, along with PIC precipitated in the fluvial system. Autochthonous POC (POC_{Auto}) and PIC (PIC_{Auto}) consist of biomass from primary productivity and carbonate particles from calcite precipitation respectively. Both types of C are sourced from the dissolved inorganic carbon (DIC) pool within the lake. Commonly, most of the DIC is atmospheric, but chemical weathering of carbonate rocks leads to the incorporation of rock-derived C into DIC (Blattmann et al., 2018; White et al., 2025). Therefore, it is important to precisely constrain the origin of DIC, as only the atmospheric fraction contributes to net atmospheric CO₂ drawdown of POC_{Auto} and PIC_{Auto}.

Several processes can influence CO₂ outgassing from the DIC pool to the atmosphere. In the past, lake metabolism, i.e., the balance between aquatic productivity and remineralization of OC, and pH-driven transformation of bicarbonate (HCO₃) to CO₂ were seen as the main drivers of CO₂ evasion (Duarte and Prairie, 2005; Many et al., 2024). However, calcite precipitation (PIC_{Auto}) is increasingly recognized as a key process inducing CO₂ outgassing (Marcé et al., 2015; Khan et al., 2022; Many et al., 2024). In lakes with alkalinity greater than 1 mM, which account for almost half of the lake surface area worldwide, alkalinity is the main source for outgassing CO₂ and consequently the process significantly influences the inland water C budget (Khan et al., 2022; Many et al., 2024). Calcite precipitation is triggered by oversaturation of lake water with respect to calcite, which can be due to warming, (re-)dissolution of calcite, a rise in pH resulting from CO₂ evasion through turbulence or CO₂ drawdown by photosynthesis, or often a combination of these processes (Khan et al., 2021). Calcite precipitation can occur at low background levels during the warm summer period or in short, distinct pulses, termed whiting events (Escoffier et al., 2022; Heine et al., 2017). The process leads to the formation of one mole of CO₂ for each mole of calcite formed, while consuming two moles of alkalinity. While the CO₂ released during calcite precipitation can be taken up by photosynthesis, calcite precipitation ultimately contributes to net CO₂ outgassing on an annual scale, by making the lake less of a CO₂ sink in summer (Many et al., 2024). The burial of calcite in sediments removes C from the active C cycle, acting as a potential sink of atmospheric CO₂. The climatic implications are further modulated by the origin of the DIC pool.

55

Radiocarbon (¹⁴C) offers a valuable tool to constrain different sources of C by utilizing the content of ¹⁴C in a sample to inform about the timing since a pool last exchanged with the atmospheric ¹⁴C pool (Graven et al., 2022; Levin and Hesshaimer, 2000; Trumbore, 2009). Pools in active exchange with the atmosphere will incorporate atmospheric ¹⁴C levels, while rock-derived

C is free of measurable ¹⁴C given its ~5700-year half-life. Pre-aged C, such as OC from soils, presents an intermediate case in this regard. DIC produced from the weathering of carbonate rocks with atmospherically-derived carbonic acid (H₂CO₃) will incorporate atmospheric and rock-derived C at equal proportions (Blattmann et al., 2018)

In this study, we determine the ¹⁴C characteristics of sinking PIC and POC from two sediment trap locations in Lake Geneva, a perialpine hardwater lake with well-documented calcite precipitation (Escoffier et al., 2023; Many et al., 2024) and considerable terrestrial C influx, the latter primarily from the upper Rhône River (Lane et al., 2019). The aim of this study is to analyze spatial and seasonal variations in the sources, fluxes and pathways of CO₂ drawdown. We compare these fluxes to those from a sediment core spanning the last ~100 years in order to assess the long-term fate of PIC and POC. We show that combined ¹⁴C measurements of both PIC and POC can be a valuable tool to precisely quantify net atmospheric CO₂ sequestration, and to highlight the potential importance of these processes with respect to the carbon balance in large, hardwater lakes.

2. Materials and Methods

2.2 Study Area

80

85

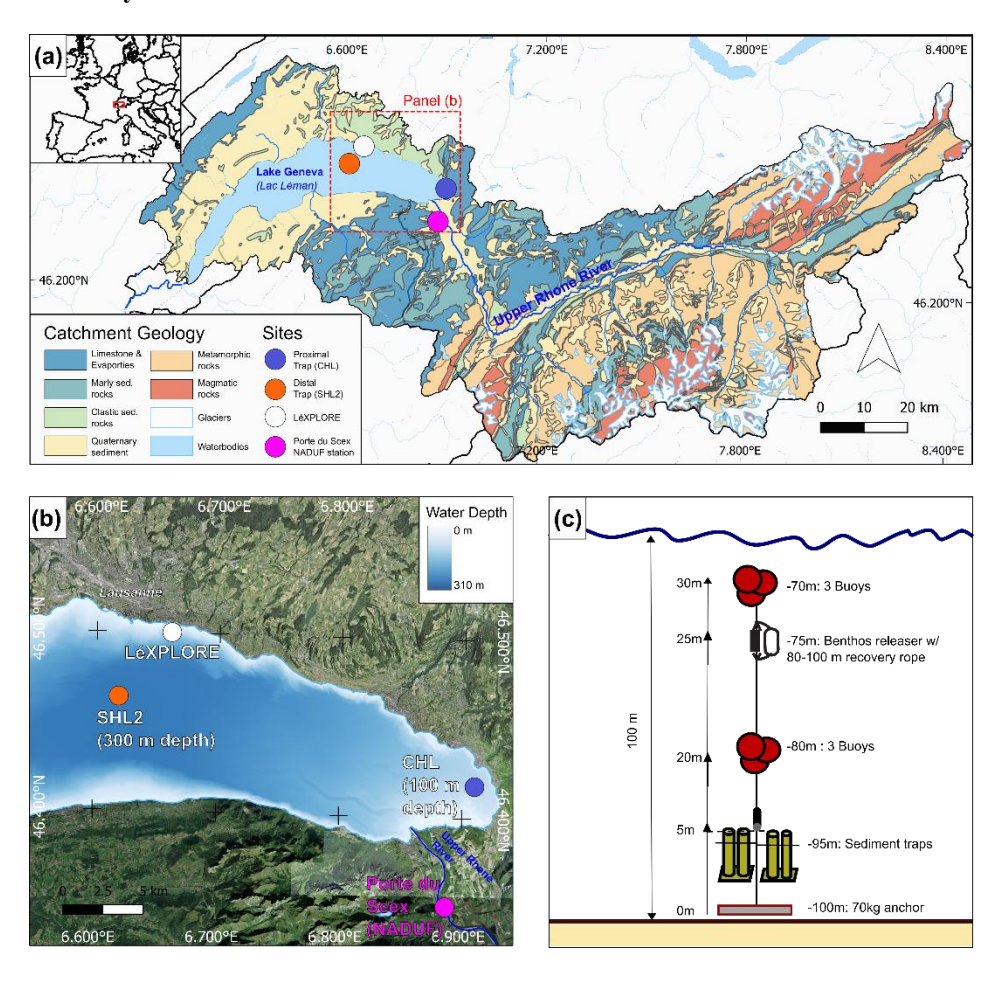


Figure 1: (a): Geological map (swisstopo, 2005) of the catchment area of Lake Geneva and sampling sites mentioned in the text. Red square indicates extent of panel (b). (b): Bathymetry (Swissbathy3D, swisstopo) of the lake and position of sampling sites. (c): Schematic setup of the sediment traps used, depth information refers to sampling site CHL. Basemaps panels (a) and (b): ESRI

Lake Geneva (Fig. 1), located between the Jura mountains to the north and the Alps to the south, has a surface area of 580 km², a maximum depth of 310 m, and a volume of 89 km³, making it the largest natural lake in Western Europe. Lake Geneva is an oligo-monomictic perialpine lake, which only mixes in very cold winters, on average every 7 years (Gaudard et al., 2017). After a period of eutrophication that peaked in the late 1970s, the lake has reached a meso-oligotrophic status with a total phosphorus (TP) concentration below 17 μg L⁻¹ (Berthon et al., 2014; Perga et al., 2016). Lake water alkalinity ranges between 1.2 and 2 mM, making it a moderately hardwater lake and reflecting the carbonate rock-rich catchment (Escoffier et al., 2023). The Upper Rhône River (Fig. 1) provides about 75-80% of the lake's inflow (Cipel, 2020) and roughly 85% of the sediment

(Loizeau et al., 2012). The river is also the primary source of phosphorous (Perga et al., 2016) and plays a key role in the sediment distribution within the lake basin (Jaquet et al., 1983). Coarser, river-derived material settles relatively close to the inflow, forming a large subaqueous delta (Silva et al., 2019; Piton et al., 2022). Finer particles are transported farther into the lake, especially due to interflow dynamics (Ishiguro and Balvay, 2003; Piton et al., 2022).

The Upper Rhône catchment consists of three major lithological units (Fig. 1a). The External Massifs in the east contain mostly granitic, magmatic rocks, the Penninic Nappes in the south comprise metamorphic and ophiolitic rocks and the Helvetic Nappes in the north consist of carbonate rocks (Schmid et al., 2004). Accordingly, provenance analyses show that the sediments transported into the lake derive about 57% from the External Massifs, 23% from Penninic Nappes, and 20% from Helvetic nappes (Stutenbecker et al., 2018). Consequently, we expect deposition of PIC_{Allo}, derived from carbonate rocks, as well as rock-derived POC, e.g., from sedimentary rocks in the Helvetic and Penninic nappes. Near the inflow, at Porte du Scex (Fig. 1(a)/(b)), a monitoring station operated by the Swiss Federal Office for the Environment (FOEN) continuously records environmental parameters of the Upper Rhône. Additionally, monitoring and research infrastructure at the *LéXPLORE* floating laboratory (Wüest et al., 2021) provide detailed insights into Lake Geneva's dynamics. This comprehensive observational network and diverse data availability make Lake Geneva an ideal environment to study C cycling processes and to apply natural isotopic tracers (esp. ¹⁴C) to delineate C sources and fates.

2.2 Sample collection

100

105

120

125

Sediment traps (Fig. 1(c)) were deployed in two locations with contrasting expected sedimentation properties. Trap CHL was deployed in a river-proximal location (~100 m depth) to capture allochthonous material emanating from the upper Rhône River. Trap SHL2 was placed at a distal location in the deepest part of the basin (~300 m depth) to capture open water sedimentation and predominantly autochthonous material. The sediment traps consisted of 4 PVC tubes each with a length of 90 cm and a diameter of 9 cm that were placed 5 m above the lake floor to ensure sinking flux to be representative of flux to the sediment. Traps were deployed on a mooring comprised of buoys, an anchor and an acoustic releaser (Fig. 1(c)) and retrieved monthly from June 2022 to June 2023 and the contents emptied into PE containers that were kept frozen until further processing. Due to disturbance of the sediment surface while deploying the distal trap for the first time in June 2022, and loss of material while retrieving the same trap in April 2023 no data is available for these periods.

Sediment cores GEN22-03 and GEN22-04 were sampled from the same location (± 300 m due to drift while sampling) as that of the proximal sediment trap CHL. The sediment cores were acquired in October 2022 using a gravity core system (Eawag-63/S corer, Eawag, Switzerland) with a 63mm PVC core liner. After sampling, sediment cores were stored at +4°C until further processing. With the available equipment, it was not possible to collect sediment cores at the distal site.

2.3 Laboratory Analyses

Sediment trap material was freeze-dried using a Christ Alpha freeze-drier and weighed to compute the sedimentation mass flux. The age-depth relationship of GEN22-04 was determined by measuring the activity of ¹³⁷Cs in the sediment core from

gamma spectroscopy on freeze-dried, homogenized samples placed into plastic tubes at the Gamma laboratory at Eawag. We analyzed 28 of these samples using high-purity Germanium Well Detectors (Canberra or Princeton Gamma-Tech). The same material was used for subsequent analysis. Sediment density was assessed from 1cm³ subsamples of the sections of GEN22-03, assuming equal core density as they were taken from the same locations and visually correlate well to one another.

We subsampled 76 sections of 1 cm thickness from GEN22-04, freeze-dried them, and weighed 2-5 g into PVC sampling tubes for bulk C analysis. We determined the organic and inorganic carbon content on 20-60 mg aliquots using a SoliTOC Cube Analyzer (Elementar GmbH, Langenselbold, Germany) at Eawag Dübendorf, determining total organic carbon (TOC) and total inorganic carbon (TIC) in weight %. We used a pure CaCO₃ standard and two standards with high and low TOC content (all provided by Säntis Analytical AG, Teufen, Switzerland) as reference materials. Standard reproducibility was better than 0.02%. For ¹⁴C measurements of PIC (PI¹⁴C), we homogenized samples with a mortar and pestle to break up aggregates and placed 3-6 mg of sample aliquots into 12 ml exetainer vials. We evacuated the headspace with ultra-high purity He, then transformed PIC into CO₂ using 85% phosphoric acid (H₃PO₄) at 60°C for 1h. The released CO₂ was introduced into the Elemental-Analyzer-Accelerator-Mass-Spectrometer (EA-AMS) MICADAS system at the Laboratory for Ion Beam Physics (LIP), ETH Zürich (Synal et al., 2007) via the Gas-Interface-System (GIS) (Mcintyre et al., 2016; Ruff et al., 2010). C1 (IAEA) was used as blank for PI¹⁴C measurements, and C2 (IAEA) as a secondary reference material.

For the analysis of Δ^{14} C and δ^{13} C of POC (PO¹⁴C and PO¹³C), 10-40 mg of sample was transferred to silver capsules (Elemental Microanalysis, 8x8x15), and inorganic C was removed by vapor acidification with 12M HCl (Bao et al., 2019; Komada et al., 2008). After neutralization with NaOH, we wrapped the samples in tin boats (Elemental Microanalysis) and measured PO¹⁴C using the MICADAS system. The standards for ¹⁴C were oxalic acid II (NIST SRM 4990C) and phthalic anhydride (Sigma, PN-320064-500g, LN-MKBH1376V). Radiocarbon measurements are reported as age corrected Δ^{14} C values in per mil (‰) (Stenström et al., 2011)

Stable δ¹³C was measured on an EA-Isotope-Ratio-Mass-Spectrometer (EA-IRMS, precisION Isoprime, Elementar GmbH, Germany). As standards for ¹³C atropine (Säntis, PN - SA990746B, LN- 51112), acetanilide (Merck, PN-100011, LN - K37102211229) and Peptone (Sigma, PN-P7750-100G, LN-SLBC5290V) were used and repeatability and intermediate precision of ¹³C measurements were better than 0.16 ‰.

2.4 Data Processing

145

150

155

Fluxes in the sediment traps were derived by weighing of the dried material. For the sediment core, we created a linear depth-density model, as well as a linear age-depth model from the measured ¹³⁷Cs peaks corresponding to 1963 (nuclear weapons tests) and 1986 (Chernobyl accident) and multiplied them into the mass accumulation rate (MAR). To identify PIC sources,

PIC_{Auto} was assumed to derive from the lake's DIC pool, while PIC_{Allo} was considered fluvially transported detrital carbonate rock devoid of measurable ¹⁴C. The relative contribution of PIC_{Auto} to total PIC flux was calculated using a two-endmember mixing model:

$$160 \quad PI^{14}C_{obs} = \alpha \times PI^{14}C_{Auto} + \beta \times PI^{14}C_{Allo} \tag{1}$$

and

165

170

175

180

$$\alpha + \beta = 1 \tag{2}$$

PI¹⁴C_{Auto} was based on DI¹⁴C data from White et al. (2025), with Δ¹⁴C values ranging from -201% to -152 %. PIC_{Allo} from the Upper Rhône River was previously estimated to be purely rock-derived based on δ^{13} C signatures (Aucour et al., 1999) and SEM microscopy of PIC (Escoffier et al., 2022). This assumption is further supported by ¹⁴C analysis of three riverine PIC samples (Appendix A) which yielded virtually ¹⁴C free results (Δ¹⁴C from -992‰ to -981‰). Consequently, PIC_{Allo} was assumed to be radiocarbon dead (-1000 %). Monte Carlo simulations (n = 100,000) were performed, drawing DI¹⁴C from a flat distribution within the observed range, as these values bound an interval without clear justification for a Gaussian distribution, and PI¹⁴C from a normal distribution centered on the observed values with their measurement uncertainties. This approach estimated the relative contributions of PIC_{Auto} and PIC_{Allo} and their associated uncertainties. For POC, the approach is less straightforward, as POC_{Allo} can display a range of ¹⁴C values (Schwab et al., 2022; Rhyner et al., 2023). Here, we used the strategic placement of the two sediment traps to resolve POC inputs - on the assumption that the river-proximal trap captures allochthonous deposition and the distal one records largely autochthonous background flux. We used the POC flux in the distal trap as a baseline of autochthonous deposition and assigned the excess POC flux in the proximal trap to allochthonous inputs. We performed all data processing and descriptive statistical analysis using Python (3.10.9) with the NumPy (1.23.5) and SciPy (1.7.3) libraries. We reconstructed the total flux for allochthonous and autochthonous POC and PIC using the results of the end member assignment in combination with the mass flux for the sediment traps. As no source apportionment has been conducted for the sediment core samples, we compare these fluxes to the bulk accumulation rates of organic and inorganic C in the sediment.

3 Results

185

200

3.1 Mass and Carbon Fluxes

The total mass flux (Fig. 2) varied markedly between the two trap locations and seasonally. In the river-proximal trap, daily mass flux varies between 2.1 g m⁻² day⁻¹ in the December 2022 deployment period to 43.7 g m⁻² day⁻¹ in the August 2022 period, with an average annual flux of 12.6 ± 12.5 g m⁻² day⁻¹. In general, lower fluvial discharge months from November to April show much lower mass flux than the months from May to October. Mass flux in the distal trap followed similar seasonal trends but was an order of magnitude lower, ranging from 0.8 g m⁻² day⁻¹ in December 2022 to 3.4 g m⁻² day⁻¹ in June 2022, averaging 1.8 ± 0.8 g m⁻² day⁻¹.

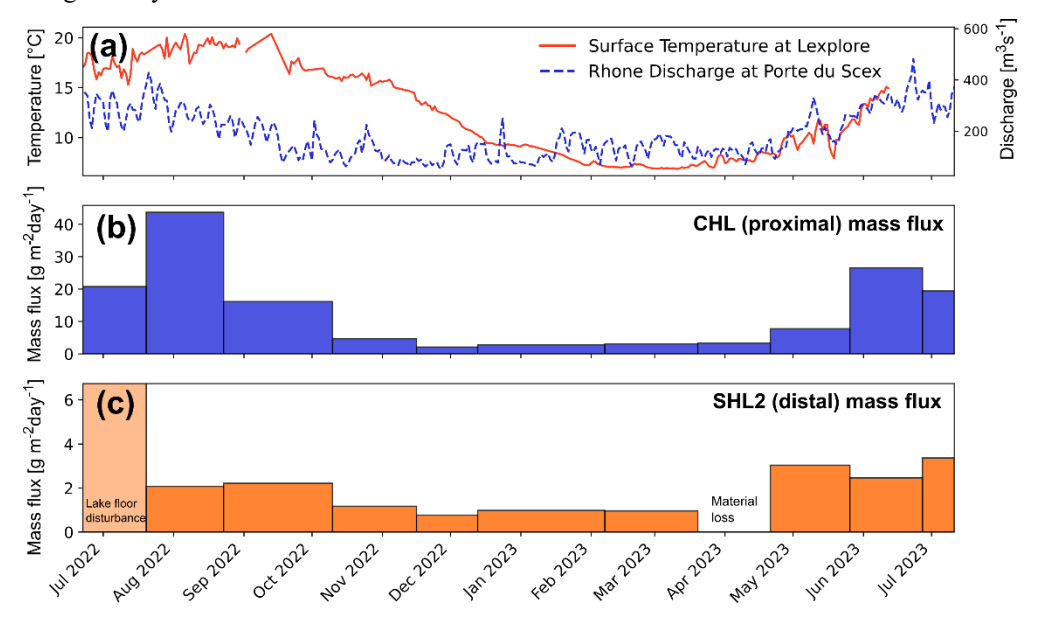
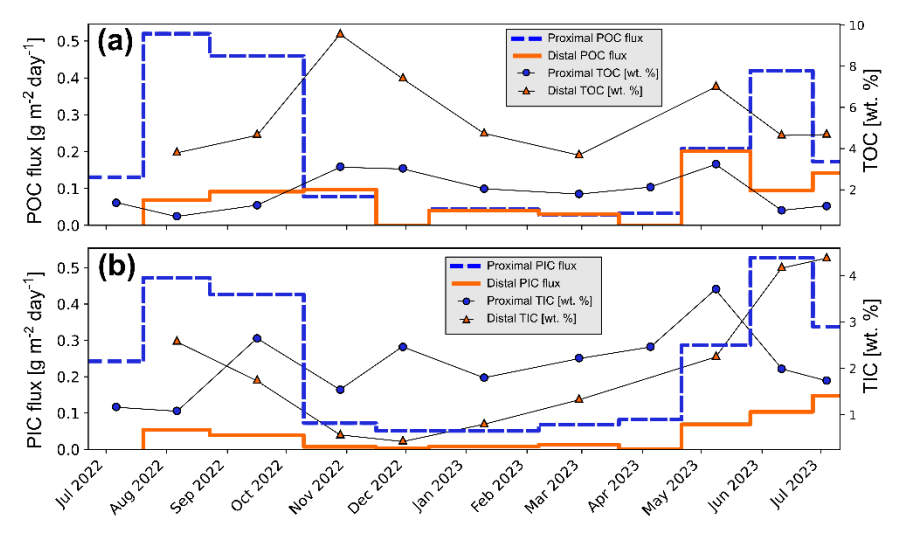


Figure 2: (a): Surface (0-20 m) water temperature (red, solid line) recorded via CTD at the LéXPLORE platform (provided by Eawag/Datalakes) and discharge (blue, dashed line) of the Upper Rhône monitored at the Porte du Scex monitoring station (provided by FOEN). (b): Mass flux in g m⁻² day⁻¹ at the proximal site (CHL). Width of the bars indicates the duration of the deployment period. (c): Mass flux in g m⁻² day⁻¹ at the distal site (SHL2). The unusually high mass flux in the first deployment period at SHL2 is attributed to sediment resuspension associated with mooring deployment. Mass flux in April at SHL2 was not quantified due to a substantial loss of material after sampling. Note the different ranges for the y-axes in panels (b) and (c).

Compared to mass flux, the flux of POC (Fig. 3(a)) shows less pronounced contrasts between the two locations. POC flux in the proximal location varies from $0.06 \text{ g m}^{-2} \text{ day}^{-1}$ in March 2023 to $0.31 \text{ g m}^{-2} \text{ day}^{-1}$ in August 2022 (annual avg., $0.17 \pm 0.10 \text{ g m}^{-2} \text{ day}^{-1}$). In the distal trap, the lowest POC flux of $0.04 \text{ g m}^{-2} \text{ day}^{-1}$ is observed in March 2023 and the maximum flux of $0.21 \text{ g m}^{-2} \text{ day}^{-1}$ is reached in May 2023 (avg., $0.10 \pm 0.05 \text{ g m}^{-2} \text{ day}^{-1}$). POC flux is comparable between the two sites from November 2022 to May 2023. The proximal trap shows higher POC flux in months with high mass flux, i.e., August to October 2022 and June-July 2023. The proportionally higher POC flux compared to mass flux in the distal trap is the result of a higher

TOC content (5.46 \pm 1.65%) relative to the proximal trap (1.31 \pm 0.72 %), which we attribute to less pronounced dilution by allochthonous lithogenic material.

Figure 3: (a): Total flux of POC in g m⁻²day⁻¹at the proximal (blue, dashed) and distal (orange, solid) site. (b): Total flux of PIC in g



205 m⁻²day⁻¹ at the proximal (blue, dashed) and distal (orange, solid) site.

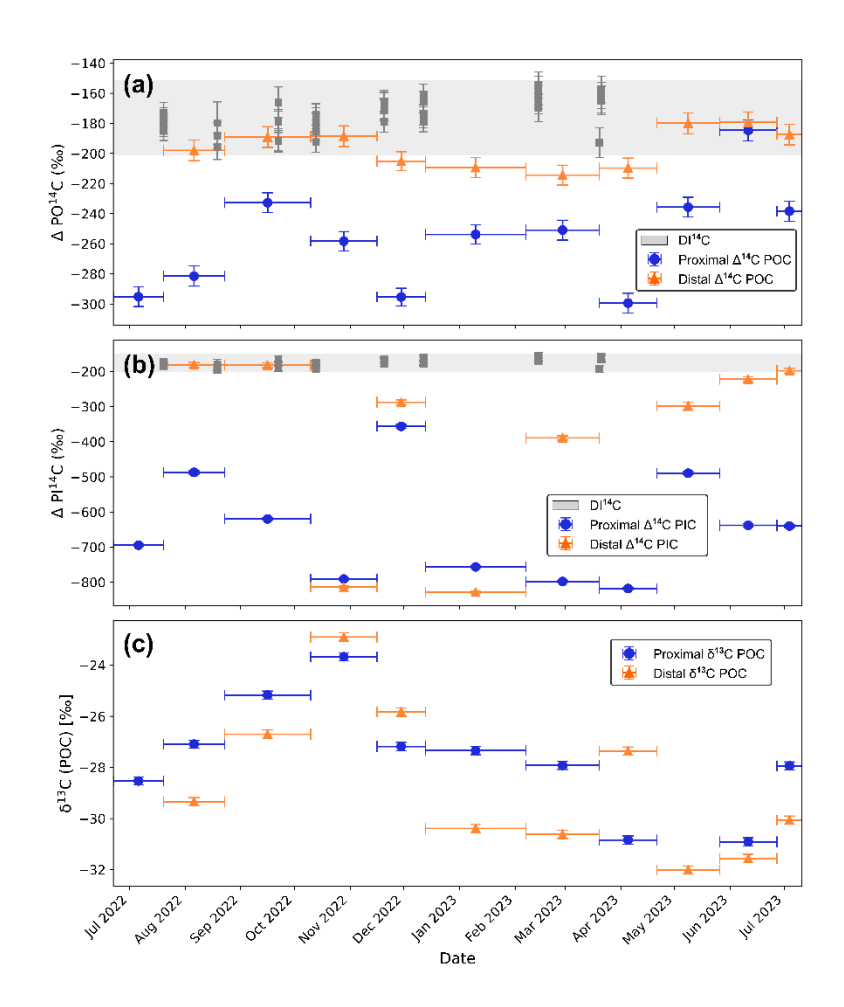
PIC fluxes fall between 0.05 g m⁻² day⁻¹ (December 2022) and 0.53 g m⁻² day⁻¹ (May 2023) in the proximal trap and between 0.01 g m⁻² day⁻¹ (October 2022) and 0.15 g m⁻² day⁻¹ (June 2023) in the distal trap. On average, the PIC flux in the proximal trap $(0.23 \pm 0.18 \text{ g m}^{-2} \text{ day}^{-1})$ is almost an order of magnitude higher than in the distal $(0.04 \pm 0.04 \text{ g m}^{-2} \text{ day}^{-1})$. This likely reflects the fact that lithogenic material contains allochthonous, detrital PIC from catchment erosion of carbonate rocks and is not, as with POC, and artifact of relative content (TIC [%]: proximal $1.80 \pm 0.74\%$ vs. distal $2.26 \pm 1.25\%$).

3.2 Carbon Isotopes and Pool-specific Fluxes

210

215

 14 C was used to assess sources of C contributing to the sediment trap fluxes at the two locations: in the distal trap, PO 14 C (Δ^{14} C values) vary from to $^{-2}$ 14 ± 7 ‰ in March 2022 to $^{-1}$ 79 ± 7 ‰ in June 2023, and average $^{-1}$ 97 ± 12 ‰ (Fig. 4a). These values are in close agreement with DI 14 C determined for the water column (White et al. (2025), suggesting that POC supply to the distal trap is dominated by autochthonous inputs. Slightly lower Δ^{14} C values of POC are reached in January to April 2023, which may reflect a higher relative contribution of allochthonous material during the colder, low-productivity period. Except for June 2023, PO 14 C values in the river-proximal trap are lower than lake DI 14 C and material in the distal trap (Fig. 4a). A detailed assessment of the 14 C signatures of POC_{Allo} is presented in Appendix A.



220 Figure 4: (a): Radiocarbon content of POC (Δ PO¹¹C) in ‰. Blue circles indicate the proximal trap, green triangles the distal trap. (b): Radiocarbon content of PIC (Δ PI¹¹C) in ‰. (c) Stable carbon isotope signature of POC (δ¹³C POC). For panel (a) & (b): The error bar in x-direction indicates the length of the deployment period. Error bars in y-direction the uncertainty of the ¹¹C measurement. The grey shaded area marks the range of values plus uncertainty observed at LéXPLORE by White et al. (2025). Grey circles mark individual observations at different water depths.

PI¹⁴C in the two traps shows much greater variability than PO¹⁴C (Fig. 4b). Δ¹⁴C values in the distal trap vary from -181 ± 7 ‰ in August 2022 to -828 ± 4 ‰ in January-February 2023 (avg., -380 ± 255 ‰). There is a clear divide into two groups: Δ¹⁴C values for the periods in November 2022 and January-February 2023 are very low (avg., -805 ± 28 ‰) while for the other periods they lie close to DI¹⁴C values (avg., -251 ± 77 ‰). PI¹⁴C in the proximal trap shows a similar pattern of variability but falls within a narrower range of Δ¹⁴C values (Fig. 4a), from -818 ‰ in April 2023 to -356 ‰ in December 2022 (avg., -257 ± 139 ‰). This least depleted period in December 2022, however, coincides with the lowest PIC flux in the time series, making the isotopic signal highly sensitive to even small variations in source contributions.

- Stable δ¹³C signatures of POC vary less strongly between the two traps, with the distal trap being slightly lower (avg. -28.7 ‰ ± 2.9 ‰) than the proximal trap (avg. -27.7 ‰ ± 2.2 ‰), likely reflecting a more autochthonous POC source at the distal site.

 Values in both traps increase from July to November 2022 before sharply decreasing, and lowest values are reached in summer 2023. In contrast to Δ¹⁴C, δ¹³C values are less diagnostic in resolving POC sources. The increasing values from July to November 2022 cannot be explained through DIC-concentration dependent fractionation, as DIC concentrations in the Lake increased during that period (White et al., 2025). Instead, changes in the composition of aquatic primary producers or increased microbial reworking due to longer residence times during convective mixing in Fall might be possible explanations.
- Assuming authigenic PI¹⁴C matches measured lake DI¹⁴C (White et al., 2025), while allochthonous PI¹⁴C is of rock-derived origin and free of measurable ¹⁴C, we determined the relative contributions of authigenic versus external sources to sedimenting PIC at both locations. In general, the relative contribution of allochthonous PIC (PIC_{Allo}) in the proximal trap (average 57% ± 17%) is higher than in the distal trap (24.56% ± 29.67%). The colder period from November to April has lower PIC fluxes and also shows the highest proportion of PIC_{Allo} in the proximal (77.90% in April 2023) and distal (79.14% in January-February 2023) traps. The highest contribution of PIC_{Auto} in the proximal trap occurred in December with 78.17%, but August 2022 and May 2023 also had high relative PIC_{Auto} fluxes (~62%). The PIC accumulating in the distal trap during summer periods (August-September 2022, June-July 2023) is almost entirely autochthonous (94-99%).

By multiplying the contribution of PIC_{Auto} with the total PIC flux, we are able to quantify the flux of PIC_{Auto} for every observation period. The flux at the two sites is generally very similar, with PIC_{Auto} flux at the proximal site only significantly exceeding that in the distal site in the summer periods of August and September 2022 and May and June 2023.

250

255

260

265

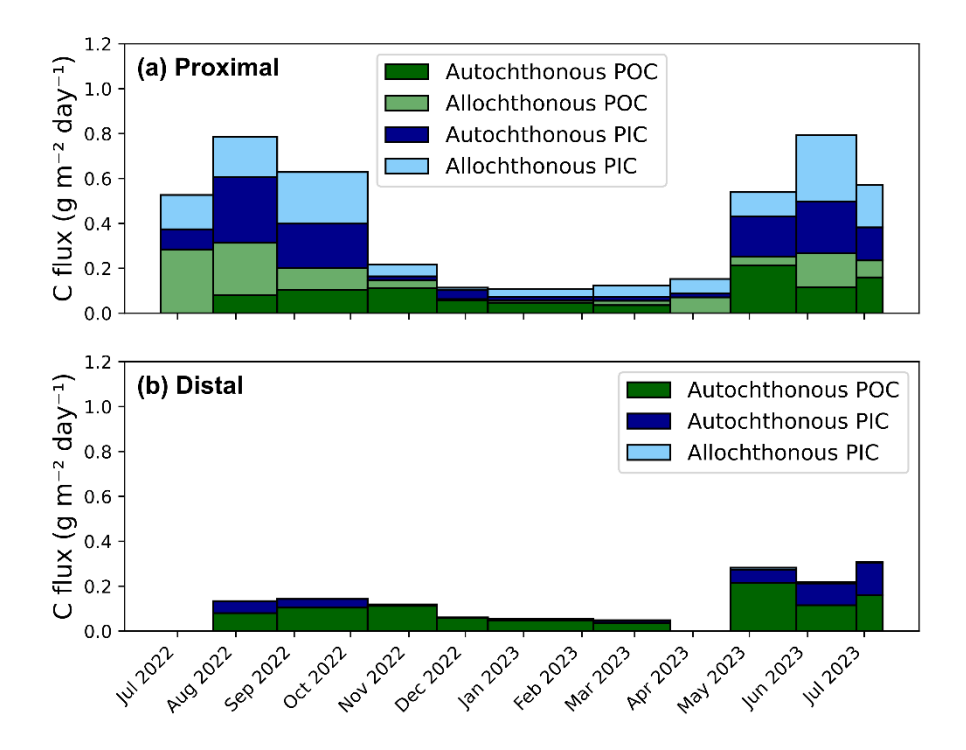


Figure 5: Modeled total annual fluxes of allochthonous and autochthonous organic and inorganic carbon for the proximal trap (a) and distal trap (b).

Over the entire observation period, overall carbon fluxes at the distal site were consistently lower than those at the proximal site (Fig. 5). At the distal site, total POC flux averaged around 0.10 ± 0.05 g m⁻² day⁻¹ and total PIC flux around 0.04 ± 0.04 g m⁻² day⁻¹. While we assigned all of the POC to be POC_{Auto} in our model, the ¹⁴C-based model predicts that the majority of PIC is also autochthonous. Consequently, seasonal trends described for total fluxes of POC and PIC apply to the autochthonous fraction. In the warmer periods, i.e., August to October 2022 and May to July 2023, POC flux is highest and deposition of PIC_{Auto} takes place, while no significant PIC accumulation is observed in winter. The total deposition at the distal location, excluding the June 2022 period (impacted by sediment disturbance) and the missing data from April 2023, is 31 g POC_{Auto} m⁻², 11.5 g PIC_{Auto} m⁻² and 1.3 g PIC_{Allo} m⁻².

In contrast, the proximal site recorded significantly higher fluxes and more mixed contributions of autochthonous and allochthonous carbon sources. For example, in August 2022, the POC flux at CHL reached 0.31 g m⁻² day⁻¹, with ~0.08 g m⁻² day⁻¹ derived from POC_{Auto} and 0.23 g m⁻² day⁻¹ from POC_{Allo}. Similarly, PIC fluxes at the proximal site were often more than an order of magnitude higher than at the distal site, peaking at 0.53 g m⁻² day⁻¹ in June 2023, with autochthonous and

allochthonous fractions frequently accounting for roughly equal proportions during high-flux periods. Deposition of PIC_{Allo} occurs mostly during the high sediment flux summer months, but steady deposition of both PIC_{Auto} and PIC_{Allo} is observed even in winter. The total annual POC flux at the proximal site is 63.7 g m⁻², comprising about 35.2 g POC_{Auto} m⁻² and 28.6 g POC_{Allo} m⁻². Note that for deployment periods without corresponding distal POC data, all POC at the proximal location was assumed to be allochthonous, potentially resulting in a slight overestimation of the POC_{Allo} contribution. The total annual PIC deposition is around 41.5 g PIC_{Auto} m⁻² and 45.8 g PIC_{Allo} m⁻².

3.3 Sediment Core

270

275

280

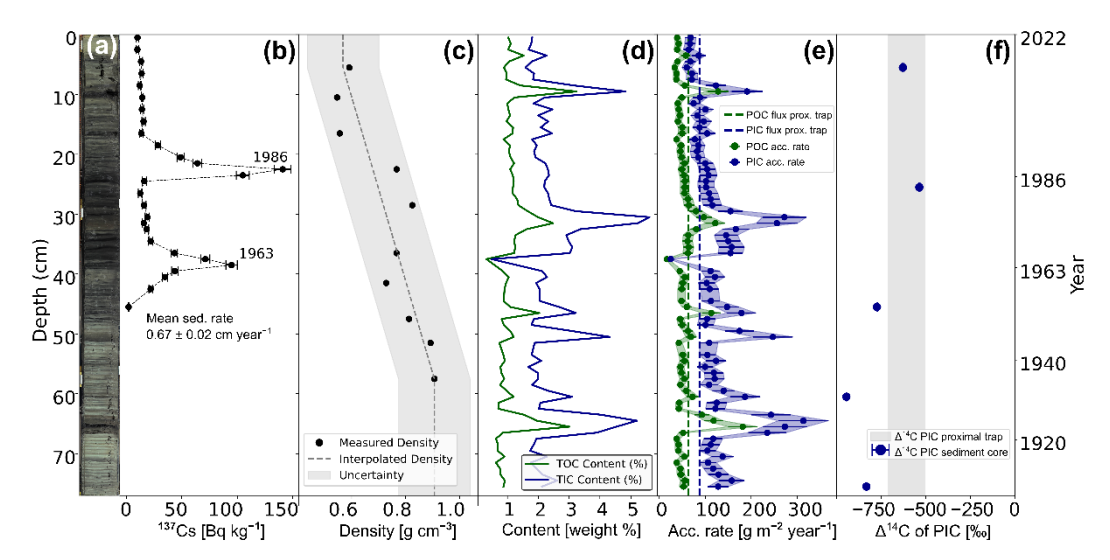
285

290

295

The sediment core sampled at the river-proximal location (Fig. 6) showed three distinct lithotypes. The top 25 cm are characterized by alternating beige-grey and dark-grey layers of 0.5 to 1 cm thickness. From 25 to 40 cm the sediment continues to show regular variations in color, but the material is dark-grey to black. We interpret this interval to coincide with the eutrophication period in the lake which occurred in the 1960s to 1980s (Jenny et al., 2016). Sediment below 40 cm consists of alternating light grey and darker grey layers. Occasionally, small turbidite layers are identified from fining-upward intervals in the sediment, e.g., at 9, 51 and 67 cm depth. Further, some very organic matter-rich, black horizons appear at 10, 25, 30 and 66 cm. Density was measured from a core sampled in the same location and visually almost identical to GEN22-04, core GEN22-03. We observed that density (Fig. 6(c)) increases from 0.6 g cm⁻³ in the top to 0.9 g m⁻³ in the lower portion of the core. This could be the result of ongoing compaction of the sediment, or stem from the slight change in facies observed in the core, or from a combination of both factors. The content of TIC and TOC (Fig. 6d) follows similar trends. TOC content is fairly constant (~1 wt.%) throughout the core, with the exception of a few depths (10, 30, 50, 65cm) where TOC increases to values of 2-3 wt.%. TIC content is around 2 wt.% throughout the core but increases in the same intervals as TOC to values up to 5 wt.%. By multiplying the TOC and TIC content with the MAR we determined the accumulation rates (AR) of PIC and POC in the core (Fig. 6(e)). When comparing this to the total flux of POC in the proximal sediment trap, we find that the AR_{POC} in the core is, in general, slightly lower than flux measured in the trap. However, in the section from 25 to 40 cm AR_{POC} exceeds fluxes from the sediment trap, before it reduces again in the lower section of the core. The peaks visible in the AR_{POC} are driven by the peaks in TOC content and should be interpreted with caution as our density model does not account for the presumably lower density of these organic-rich layers. In the top portion of the core, AR_{PIC} follows similar patterns as AR_{POC} being first slightly lower than in the trap and exceeding it in the 25-40 cm interval. In the lower portion however, AR_{PIC} increases even more. The latter potentially reflects a higher content in detrital PIC in these visibly lighter facies. PI¹⁴C in the sediment (Fig. 6(f)) ranges from $-946 \pm 1\%$ at 60 cm depth to $-536 \pm 4\%$ at 25 cm. Values in the higher portion of the core agree with the mean PI14C signature of the proximal sediment trap, while values in the bottom section of the core are lower, consistent with a higher detrital contribution in this part. However, values are far from radiocarbon-dead, e.g., $-834 \pm 2\%$ at 75 cm depth, underlining the significant contribution of authigenic calcite even at depth.

Figure 6: (a): Line scan photograph of core GEN22-04, (b): Activity of ¹³⁷Cs in GEN22-04, two maxima in 23 and 39 cm depth are assigned to 1986 (Chernobyl disaster) and 1963 (nuclear weapons tests) respectively. (c): Dry bulk density of GEN22 -03 as determined with a volumetric sampler. A linear model is fit to the observed data, constant values assumed for depth above and below



measured data. (d): Content of TIC (blue) and TOC (green) in weight % in core GEN22-04, (e): Mass accumulation rate of PIC (blue) and POC (green) in GEN22-04. Uncertainty in shaded blue/green. Dashed lines indicate total annual deposition of PIC (blue) and POC (green) in the proximal sediment trap. (f): Radiocarbon content of PIC (\$\Delta\$ PI\$\$\subseteq\$ (\$\Delta\$ PI\$\$\subseteq\$ (\$\Delta\$ lines in the core GEN22-04 (blue dots). Shaded grey area shows mean and standard deviation of the average PI\$\$\subseteq\$ 10 fthe proximal sediment trap.

4 Discussion

305

310

315

300

4.1 Controls on POC Flux

Accumulation of POC in Lake Geneva reflects the complex interactions between allochthonous inputs from the Upper Rhône River and autochthonous production within the lake. This study sheds light on the spatial and seasonal variability in POC fluxes, driven by hydrological and biological processes, as well as the preservation dynamics observed in underlying sediments. Total mass flux as well as POC flux were consistently higher in the proximal compared to the distal trap, especially in the warmer months. We interpret this to be the result of increased fluvial discharge in spring and summer when meltwater influx increases, and rainfall events occur. Mass and POC flux in the proximal trap illustrate how increased Upper Rhône discharge delivers large quantities of terrestrial material and associated OC. In August and September 2022, POC flux in the proximal trap was nearly three times as high as in the distal trap, underlining the dominant role of fluvial input on POC flux during these periods. In contrast, POC fluxes in both traps were comparable during colder, low-discharge periods (November 2022 to April 2023) as a consequence of the reduced supply of fluvial material. These trends are also illustrated by PO 14 C. Δ^{14} C values in the distal trap lie consistently within, or close to the observed range of DI 14 C, indicating a dominance of POC_{Auto}, whereas the proximal trap exhibits lower Δ^{14} C values that reflect input of pre-aged POC_{Allo} from the catchment, especially during high-discharge periods. This interpretation is further supported by the δ^{13} C values (< -28 % in most periods) in the

distal trap, characteristic of lacustrine organic matter (Randlett et al., 2015). Furthermore, the higher TOC content in the distal trap $(5.46 \pm 1.65 \%)$ compared to the proximal trap $(1.31 \pm 0.72 \%)$ reflects the less pronounced dilution by lithogenic material and the dominance of POC_{Auto} at the distal site.

In addition to the riverine input, the relative contributions of POC_{Allo} and POC_{Auto} are influenced by in-lake primary productivity. During periods of high productivity, such as May 2023, as recorded by chlorophyll a monitoring at LéXPLORE (Datalakes/EAWAG), the distal trap recorded its highest POC flux, while the proximal trap continued to exhibit aged PO¹⁴C (lower Δ^{14} C) signatures, suggesting concurrent inputs of autochthonous POC and terrestrial material. This complex interplay between external influx and internal productivity was apparent in June 2023. Despite similar Δ^{14} C values of POC and DIC, the proximal trap recorded nearly twice the POC flux compared to the distal trap. This could be the result of higher autochthonous POC deposition in the proximal trap, influenced by nutrient delivery from the river (Cotte et al., 2023; Kiefer et al., 2015). Alternatively, it could be caused by the influx of POC_{Allo} with a 14 C signature similar to that of DI¹⁴C, which is possible, given the average PO¹⁴C of Swiss rivers was -164‰ in Summer 2021 (Rhyner et al., 2023). Further studies are required to resolve this question, but we note that POC_{Auto} deposition in the proximal site may be slightly underestimated.

Insights into long-term POC burial are provided by sediment core GEN22-04. The top 25 cm of the core revealed lower AR_{POC} compared to fluxes in the proximal trap, likely reflecting ongoing decomposition of POC following arrival at the sediment-water interface. During the eutrophic interval (25–40 cm depth), AR_{POC} exceeded trap fluxes, coinciding with periods of heightened productivity (Loizeau and Dominik, 2005). In the deeper sections of the core (>40 cm), AR_{POC} values decreased, approaching trap flux levels, suggesting effective preservation of POC, likely due to rapid burial and reduced remineralization in this high sedimentation deltaic site (Randlett et al., 2015; Sobek et al., 2009). The variability of TOC content (maxima of 2–3 wt.%), within the sediment core is primarily driven by short-term fluctuations that we interpret to be either linked to high-productivity events such as algal blooms or the influx of organic-rich terrestrial material. Concurrent increases in both TIC and TOC suggest a coupling between productivity and PIC deposition, as has been observed previously (Dittrich and Obst, 2004; Escoffier et al., 2023). However, it must be noted that our density model likely overestimates AR_{POC} in these organic-rich layers due to the unaccounted lower sediment density.

4.2 Controls on PIC Flux

325

330

335

340

PIC fluxes in Lake Geneva feature pronounced seasonal variability and contrasts between the proximal and distal locations. In general, PIC sedimentation is influenced by the interplay between allochthonous supply of detrital material and autochthonous calcite precipitation. The proximal trap consistently recorded higher PIC fluxes compared to the distal trap throughout all sampling periods, while seasonal variability, driven by hydrology and productivity, significantly influenced the relative contributions of PIC_{Auto} and PIC_{Allo}. The distal trap predominantly recorded PIC_{Auto}, whereas the proximal trap exhibited significant contributions of PIC_{Allo} material, especially during the high-discharge summer months.

At the distal site, PIC fluxes were almost entirely autochthonous, with PI¹⁴C values closely matching those of DI¹⁴C in most months. This pattern reflects the location, far from the riverine influence, and the dominance of calcite precipitation linked to in-lake primary productivity. However, during a few periods (e.g., November 2022 and January–February 2023), PI¹⁴C values indicated the co-deposition of allochthonous detrital carbonate. This increase in PIC_{Allo} deposition could be linked to resuspension and lateral transport of (deltaic) sediment following enhanced bottom boundary layer turbulence during convective mixing in fall/winter (Fernández Castro et al., 2021). Given the overall low PIC flux in these months, even a small contribution of PIC_{Allo} was sufficient to produce the observed ¹⁴C-depleted signatures.

At the proximal site, PIC_{Allo} deposition was more prevalent, especially during the summer, when high river-discharge led to high input of sediment, including detrital carbonates (PIC_{Allo}). However, the proximal site also exhibited a higher flux of PIC_{Auto} than the distal one. We identify two processes that may account for this contrast: (1) The shallower depth and thus shorter residence time in the water column at the proximal site might enhance preservation of PIC_{Auto}. (2) The calcite precipitation in the proximal site could be higher than in the distal site. As calcite precipitation is closely tied to primary productivity in the lake (Many et al., 2024) and the river is the main source of nutrients (Kiefer et al., 2015; Cotte et al., 2023), the Upper Rhône discharge might fuel productivity in the proximal site, leading to increased PIC_{Auto} precipitation. Further, suspended particles of detrital carbonate, which are more abundant in this location, have been identified as important nucleation sites for calcite precipitation in Lake Geneva (Escoffier et al., 2023), and are linked to occurrence of whiting events in the delta region (Escoffier et al., 2022).

Water-column dissolution of calcite particles in Swiss hardwater lakes is minimal, and dissolution rather occurs in the shallow sediment—water interface, driven by pH changes through organic matter decomposition (Müller et al., 2016; Müller et al., 2006). Consequently, our deep sediment traps provide accurate estimates of PIC flux to the sediment. Sediment core GEN22-04 then provides additional insights into long-term PIC accumulation and preservation. In the upper core section, AR_{PIC} values were slightly lower than fluxes observed in the proximal trap, suggesting ongoing dissolution of PIC, although we cannot rule out potentially higher PIC flux in the studied year compared to previous ones. However, the eutrophic interval (approximately 25–40 cm depth) exhibited increased PIC deposition, consistent with the enhanced primary productivity observed during that period. This pattern highlights the link between calcite precipitation and biological productivity. PI¹⁴C in the top section of the core as well as during the eutrophic period agree with the mean values recorded by our sediment trap, suggesting ongoing deposition and preservation of the authigenic calcite. Importantly, the eutrophic interval coincides with the manifestation of the atmospheric bomb spike in the DI¹⁴C (Mittelbach et al., 2025) and slightly elevated values do not necessarily reflect more authigenic PIC. In the lower portion of the core (below 40 cm), non radiocarbon-dead PI¹⁴C signatures show a persistent flux of authigenic calcite, despite changes in sediment facies indicating a shift in depositional conditions. This interval, deposited before approximately 1960, predates significant hydrological interventions in the Upper Rhône catchment, including dam construction and channelization (Lane et al., 2019). We interpret this section to be dominated by detrital PIC, reflecting greater

delivery of carbonate-rich sediments from the catchment rather than increased PIC_{Auto} precipitation. The Δ PI¹⁴C of $-834 \pm 2\%$ in the deepest sample would indicate ~20% of the PIC flux being authigenic assuming DI¹⁴C to be similar as today. In summary, despite the evidence for carbonate dissolution in the upper core, our findings suggest good preservation of autochthonous PIC in the deltaic site overall. This observation contrasts with modeling studies (e.g., Many et al., 2024) that predict complete dissolution of PIC_{Auto} based on the lake's Ca²⁺ budget. At least in the deltaic region, significant fractions of autochthonous calcite appear to be retained in the sediment, underlining the importance of site-specific conditions in determining PIC preservation.

4.3 Ramifications for the freshwater C sink

385

390

395

400

405

Using our point observations, we can derive first-order estimates of carbon fluxes for the different pools across the lake. PIC_{Auto} flux ranged from approximately 40 g m⁻² yr⁻¹ in the proximal site to 12 g m⁻² yr⁻¹ in the distal site, corresponding to an extrapolated 7–30 Gg C yr⁻¹ if extended over the entire lake. The lower bound of ~7 Gg C yr⁻¹ should be considered conservative as it is based on the observations from the deepest site of the lake and calcite burial tends to be higher in shallower waters. Assuming that the deltaic sedimentation zone, with higher authigenic calcite flux, accounts for roughly 15% of the lake (Jaquet et al., 1983) yields a more realistic basin-wide estimate of about 10 Gg C yr⁻¹. By comparison, ~17 Gg of calcite is modeled to precipitate annually (Many et al., 2024), indicating relatively effective burial of these particles. Although the long-term fate of PIC_{Auto} in most parts of the lake remains unknown, our sediment core data indicates that the 3.5 Gg yr⁻¹ deposited in the deltaic zone are likely to be preserved. Radiocarbon analyses allow us to distinguish this from the 6.5 (3–25) Gg C yr⁻¹ of PIC_{Allo} deposited in the lake.

Projecting POC_{Auto} burial from the distal site to the entire lake suggests 20 Gg C yr⁻¹, of which ~3 Gg C yr⁻¹ are buried in the delta. Current estimates indicate that ~8% of the NEP (8 Gg C yr⁻¹) are buried annually (Steinsberger et al., 2021). Coupled with the ongoing POC decomposition in the sediment (Steinsberger et al., 2021), this implies that the distal trap's flux may not represent the final burial flux. Our data indicate that POC_{Allo} accumulation in the delta sums to ~16 Gg C yr⁻¹, consistent with an estimated 14 Gg C yr⁻¹ of Rhône-derived TOC input in 1974–2010 (Rodriguez-Murillo and Filella, 2015). This agreement suggests that our chosen proximal site is broadly representative of deltaic burial fluxes. Preservation of POC_{Allo} in deltaic sediments is known to be efficient (Mittelbach et al., 2025; Sobek et al., 2009; Randlett et al., 2015). Overall, these findings illustrate that, despite their limited spatial coverage, data from our sediment trap deployments provide robust estimates of depositional fluxes for individual carbon pools in Lake Geneva.

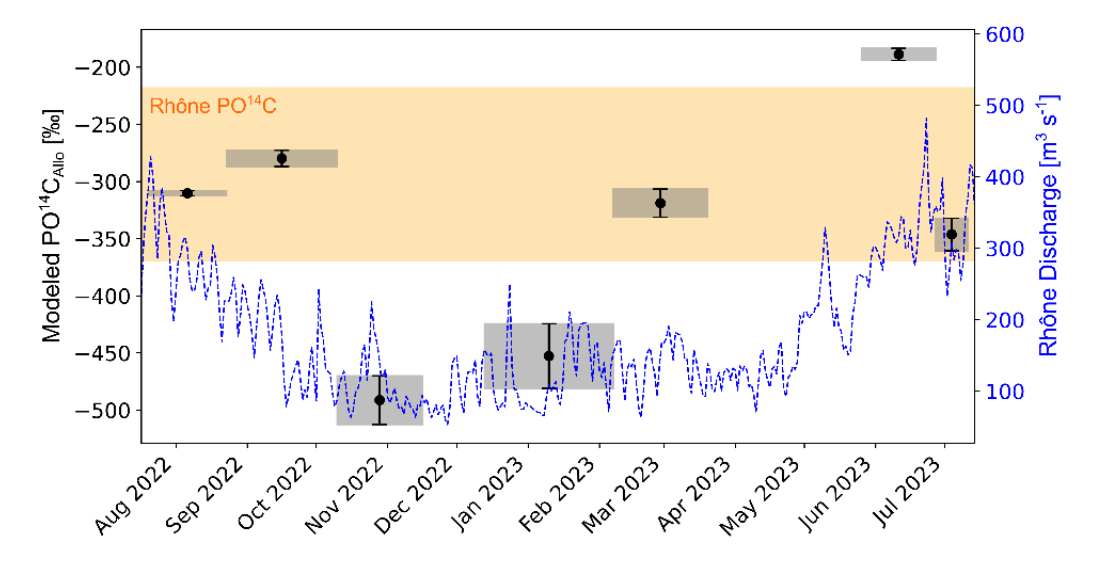
410 5 Conclusions

By analyzing POC and PIC sources in two sediment traps in Lake Geneva, we were able to show that calcite precipitation can be an important contribution to C sequestration in this and other hardwater lakes. ¹⁴C measurements enabled us to distinguish between external and internal PIC. In the subaqueous delta region, the observed authigenic PIC fluxes were four times higher

than in the distal sediment trap. Furthermore, analysis of a sediment core from the delta revealed that this authigenic PIC is at least partially preserved in the sediment. This challenges model predictions of complete dissolution and highlights the importance of calcite precipitation in hardwater lakes not only as a driver of CO₂ outgassing, but also as an under-recognized burial flux of carbon. Although sediment traps can only provide localized, short-term data, measured C fluxes are in agreement with existing, independent observations, and with data from longer-term sediment archives. Building on this work, future research should include broader spatial coverage to refine estimates for the entire lake, more detailed sampling of sediment cores to analyze the long-term fate of deposited POC and PIC in Lake Geneva, and extension to other hardwater lake systems.

Appendix A: Radiocarbon Signatures of Allochthonous PIC and POC

By comparing the different PO¹⁴C signatures between the two traps, we estimated the PO¹⁴C_{Allo}. To avoid unrealistic results (i.e., very low PO¹⁴C_{Allo}), we only applied this approach for months where the POC flux of the proximal trap exceeded that of the distal trap by at least 20%. This criterion yielded seven valid periods (August to November 2022; January to March, and June and July 2023). We applied Monte-Carlo simulations (n = 100,000) to account for uncertainties in the ¹⁴C measurements. By using the POC flux in the distal trap as an autochthonous baseline and assigning the excess POC flux in the river-proximal trap as allochthonous, we were able to calculate the PO¹⁴C signature of this allochthonous fraction. The highest Δ^{14} C value of POC_{Allo} was reached in June 2023 with -189 ‰ ± 5 ‰, while the lowest PO¹⁴C_{Allo} signature occurs in the November 2022 with -491 ‰ ± 21 ‰ (Fig. A1). The average PO¹⁴C_{Allo} is-341 ‰ ± 103 ‰, or -294 ‰ ± 48 ‰ when using an average weighted for individual uncertainty. These values are in agreement with observations for riverine suspended PO¹⁴C by Rhyner et al. (2023) who reported -218‰ ± 7‰ for Summer 2021 and -369 ± 7‰ for Summer 2022; the latter was measured as part of this study using the sampling and measuring protocol outlined in Rhyner et al. (2023). Increased Upper Rhône discharge appears to



coincide with younger POC_{Allo}, as has been observed in other Swiss mountainous rivers (Gies et al., 2022; Schwab et al., 2022), but no statistically significant relationship emerges. The March 2023 period deviated from this trend, illustrating the inherent variability of riverine PO¹⁴C. These large variations within a single year underscore the need for long-term, high-resolution monitoring to accurately constrain fluvial PO¹⁴C sources and export.

Figure A1: Modeled ¹⁴C signature of allochthonous POC in the proximal trap for periods with POC flux more than 20% higher than in the distal trap. Grey are shows standard deviation as determined by Monte-Carlo simulations. Dashed blue line shows discharge data of the Rhône River at Porte du Scex provided by the Swiss Federal Office for the Environment (FOEN). Shaded orange zone shows range of measures upper Rhône PO¹⁴C by Rhyner et al. (2023).

To better constrain the riverine PIC endmember, we analyzed the PI¹⁴C signature of three Rhône River suspended sediment samples, collected ant the Porte du Scex NADUF station in Summer 2023, Spring 2023 and Summer 2021, using the protocol described by (Rhyner et al., 2023). All samples gave virtually ¹⁴C free results with Δ^{14} C of –992 ± 1 ‰ (July 2023), –985 ± 1 ‰ (April 2023), and –981 ± 1 ‰ (July 2021).

Acknowledgments

435

445

450

455

460

We thank Sébastien Lavanchy and Guillaume Cunillera (EPFL/LéXPLORE) and Anita Schlatter (Eawag) for organizing and facilitating field sampling. We acknowledge the technical and administrative support of the entire LéXPLORE team and the five LéXPLORE partner institutions: Eawag, EPFL, University of Geneva, University of Lausanne, and CARRTEL (INRAE–USMB). We are grateful to Alexander Brunmayr, Sarah Paradis, Remo Röthlin, Madeleine Santos, Charlotte Schnepper, and Aline Wildberger for field assistance. We thank Pascal Rünzi (Eawag) for gamma spectroscopy and Marcel Walter (Eawag) for SoliTOC measurements. AMS measurements were supported by the Laboratory of Ion Beam Physics at ETH Zurich. We also thank all contributors to the Radiocarbon Inventories of Switzerland project. We used ChatGPT (OpenAI) and Grammarly (Grammarly Inc.) to enhance writing clarity and assist with Python coding. This work was funded by the Swiss National Science Foundation Sinergia Grant No. 193770.

Author Contributions

BVAM led the conceptualization and design of the study with contributions from TIE and ND. Method development was carried out by BVAM, MEW, and NH. BVAM implemented the software and performed data curation and formal analysis with input from MEW, MEP, and NH. Field investigation was conducted by BVAM and MEW. Resources were provided by TIE and ND. BVAM wrote the original draft of the manuscript with contributions from TIE, MEW, MEP, and ND. All authors contributed to review and editing. Visualization was prepared by BVAM. Project supervision and administration were carried out by ND and TIE, who also acquired funding for the study.

Data Availability

All data presented in this study as well as code required to reproduce the results is on Zenodo at doi.org/10.5281/zenodo.15102592. All data from the ongoing monitoring at the LéXPLORE platform is openly available at www.datalakes-eawag.ch.

References

505

- Aucour, A.-M., Sheppard, S. M., Guyomar, O., and Wattelet, J.: Use of 13C to trace origin and cycling of inorganic carbon in the Rhône river system, Chemical Geology, 159, 87-105, 1999.
- 470 Bao, R., McNichol, A. P., Hemingway, J. D., Gaylord, M. C. L., and Eglinton, T. I.: Influence of different acid treatments on the radiocarbon content spectrum of sedimentary organic matter determined by RPO/accelerator mass spectrometry, Radiocarbon, 61, 395-413, 2019.
 - Berthon, V., Alric, B., Rimet, F., and Perga, M. E.: Sensitivity and responses of diatoms to climate warming in lakes heavily influenced by humans, Freshwater Biology, 59, 1755-1767, 2014.
- Blattmann, T. M., Wessels, M., McIntyre, C. P., and Eglinton, T. I.: Projections for Future Radiocarbon Content in Dissolved Inorganic Carbon in Hardwater Lakes: A Retrospective Approach, Radiocarbon, 60, 791-800, 10.1017/rdc.2018.12, 2018. CIPEL: Rapp. Comm. int. pour la protec. des eaux du Léman contre la pollution, Campagne 2019, Agroscope - Changins - Bâtiment DC, Nyon, 2020.
- Cole, J. J., Prairie, Y. T., Caraco, N. F., McDowell, W. H., Tranvik, L. J., Striegl, R. G., Duarte, C. M., Kortelainen, P., Downing, J. A., and Middelburg, J. J.: Plumbing the global carbon cycle: integrating inland waters into the terrestrial carbon budget, Ecosystems, 10, 172-185, 2007.
 - Cotte, G., Soulignac, F., dos Santos Correia, F., Fallet, M., Ibelings, B. W., Barry, D. A., and Vennemann, T. W.: Controlling factors of phytoplankton distribution in the river–lake transition zone of a large lake, Aquatic Sciences, 85, 37, 2023.
- Dittrich, M. and Obst, M.: Are picoplankton responsible for calcite precipitation in lakes?, AMBIO: A Journal of the Human Environment, 33, 559-564, 2004.
 - Duarte, C. M. and Prairie, Y. T.: Prevalence of heterotrophy and atmospheric CO 2 emissions from aquatic ecosystems, Ecosystems, 8, 862-870, 2005.
 - Eglinton, T. I., Galy, V. V., Hemingway, J. D., Feng, X., Bao, H., Blattmann, T. M., Dickens, A. F., Gies, H., Giosan, L., Haghipour, N., Hou, P., Lupker, M., McIntyre, C. P., Montlucon, D. B., Peucker-Ehrenbrink, B., Ponton, C., Schefuss, E.,
- Schwab, M. S., Voss, B. M., Wacker, L., Wu, Y., and Zhao, M.: Climate control on terrestrial biospheric carbon turnover, Proc Natl Acad Sci U S A, 118, 10.1073/pnas.2011585118, 2021.
 - Escoffier, N., Perolo, P., Many, G., Pasche, N. T., and Perga, M.-E.: Fine-scale dynamics of calcite precipitation in a large hardwater lake, Science of The Total Environment, 864, 160699, 2023.
- Escoffier, N., Perolo, P., Lambert, T., Rüegg, J., Odermatt, D., Adatte, T., Vennemann, T., and Perga, M. E.: Whiting events in a large peri-alpine lake: Evidence of a catchment-scale process, Journal of Geophysical Research: Biogeosciences, 127, e2022JG006823, 2022.
 - Fernández Castro, B., Chmiel, H. E., Minaudo, C., Krishna, S., Perolo, P., Rasconi, S., and Wüest, A.: Primary and net ecosystem production in a large lake diagnosed from high-resolution oxygen measurements, Water Resources Research, 57, e2020WR029283, 2021.
- Gaudard, A., Schwefel, R., Vinnå, L. R., Schmid, M., Wüest, A., and Bouffard, D.: Optimizing the parameterization of deep mixing and internal seiches in one-dimensional hydrodynamic models: a case study with Simstrat v1. 3, Geoscientific Model Development, 10, 3411-3423, 2017.
 - Gies, H., Lupker, M., Wick, S., Haghipour, N., Buggle, B., and Eglinton, T.: Discharge-Modulated Soil Organic Carbon Export From Temperate Mountainous Headwater Streams, Journal of Geophysical Research: Biogeosciences, 127, 10.1029/2021jg006624, 2022.
 - Graven, H., Keeling, R., and Xu, X.: Radiocarbon dating: going back in time, Nature, 607, 449-449, 2022.

- Heine, I., Brauer, A., Heim, B., Itzerott, S., Kasprzak, P., Kienel, U., and Kleinschmit, B.: Monitoring of calcite precipitation in hardwater lakes with multi-spectral remote sensing archives, Water, 9, 15, 2017.
- Ishiguro, N. and Balvay, G.: L'écoulement des eaux du Rhône dans le lac Léman, Archives des sciences, 56, 117-126, 2003.
- Jaquet, J.-M., Rapin, F., Davaud, E., and Vernet, J.-P.: Géochimie des sédiments du Léman, 1983.

 Jenny, J.-P., Normandeau, A., Francus, P., Taranu, Z. E., Gregory-Eaves, I., Lapointe, F., Jautzy, J., Ojala, A. E., Dorioz, J.-M., and Schimmelmann, A.: Urban point sources of nutrients were the leading cause for the historical spread of hypoxia across European lakes. Proceedings of the National Academy of Sciences, 113, 12655-12660, 2016.
- Khan, H., Marcé, R., Laas, A., and Obrador Sala, B.: The relevance of pelagic calcification in the global carbon budget of lakes and reservoirs, Limnetica, 2022, vol. 41, 2022.
 - Khan, H., Laas, A., Marcé, R., Sepp, M., and Obrador, B.: Eutrophication and geochemistry drive pelagic calcite precipitation in lakes, Water, 13, 597, 2021.
 - Kiefer, I., Odermatt, D., Anneville, O., Wüest, A., and Bouffard, D.: Application of remote sensing for the optimization of insitu sampling for monitoring of phytoplankton abundance in a large lake, Science of the Total Environment, 527, 493-506, 2015.
 - Komada, T., Anderson, M. R., and Dorfmeier, C. L.: Carbonate removal from coastal sediments for the determination of organic carbon and its isotopic signatures, δ13C and Δ14C: comparison of fumigation and direct acidification by hydrochloric acid, Limnology and Oceanography: Methods, 6, 254-262, 2008.

520

- Lane, S. N., Bakker, M., Costa, A., Girardelos, S., Loizeau, J.-L., Molnar, P., Silva, T., Stutenbecker, L., and Schlunegger, F.:
- Making stratigraphy in the Anthropocene: climate change impacts and economic conditions controlling the supply of sediment to Lake Geneva, Scientific reports, 9, 8904, 2019.

 Levin, I. and Hesshaimer, V.: Radiocarbon–a unique tracer of global carbon cycle dynamics, Radiocarbon, 42, 69-80, 2000.
 - Loizeau, J.-L. and Dominik, J.: The history of eutrophication and restoration of Lake Geneva, Terre Environ, 50, 43-56, 2005. Loizeau, J.-L., Girardclos, S., and Dominik, J.: Taux d'accumulation de sédiments récents et bilan de la matière particulaire
- dans le Léman (Suisse-France), Arch. Sci, 65, 81-92, 2012.
 Many, G., Escoffier, N., Perolo, P., Bärenbold, F., Bouffard, D., and Perga, M.-E.: Calcite precipitation: The forgotten piece of lakes' carbon cycle, Science Advances, 10, eado5924, 2024.
 - Marcé, R., Obrador, B., Morguí, J.-A., Lluís Riera, J., López, P., and Armengol, J.: Carbonate weathering as a driver of CO2 supersaturation in lakes, Nature Geoscience, 8, 107-111, 2015.
- McIntyre, C. P., Wacker, L., Haghipour, N., Blattmann, T. M., Fahrni, S., Usman, M., Eglinton, T. I., and Synal, H.-A.: Online 13C and 14C Gas Measurements by EA-IRMS-AMS at ETH Zürich, Radiocarbon, 59, 893-903, 10.1017/rdc.2016.68, 2016. Mittelbach, B. V., Brunmayr, A., White, M. E., Rhyner, T. M., Haghipour, N., Blattmann, T. M., Wessels, M., Dubois, N., and Eglinton, T. I.: Pre-aged organic matter dominates organic carbon burial in a major perialpine lake system, Limnology and Oceanography, 00, 1-13, doi: 10.1002/lno.12815, 2025.
- 540 Müller, B., Meyer, J. S., and Gächter, R.: Alkalinity regulation in calcium carbonate-buffered lakes, Limnology and Oceanography, 61, 341-352, 2016.
 - Müller, B., Wang, Y., and Wehrli, B.: Cycling of calcite in hard water lakes of different trophic states, Limnology and Oceanography, 51, 1678-1688, 2006.
- Perga, M.-E., Maberly, S. C., Jenny, J.-P., Alric, B., Pignol, C., and Naffrechoux, E.: A century of human-driven changes in the carbon dioxide concentration of lakes, Global Biogeochemical Cycles, 30, 93-104, 10.1002/2015gb005286, 2016.
- Piton, V., Soulignac, F., Lemmin, U., Graf, B., Wynn, H. K., Blanckaert, K., and Barry, D. A.: Tracing unconfined nearfield spreading of a river plume interflow in a large Lake (Lake Geneva): Hydrodynamics, suspended particulate matter, and associated fluxes, Frontiers in Water, 4, 943242, 2022.
- Randlett, M. E., Sollberger, S., Del Sontro, T., Muller, B., Corella, J. P., Wehrli, B., and Schubert, C. J.: Mineralization pathways of organic matter deposited in a river-lake transition of the Rhone River Delta, Lake Geneva, Environ Sci Process Impacts, 17, 370-380, 10.1039/c4em00470a, 2015.
 - Rhyner, T. M., Bröder, L., White, M. E., Mittelbach, B. V., Brunmayr, A., Hagedorn, F., Storck, F. R., Passera, L., Haghipour, N., and Zobrist, J.: Radiocarbon signatures of carbon phases exported by Swiss rivers in the Anthropocene, Philosophical Transactions of the Royal Society A, 381, 20220326, 2023.
- Rodriguez-Murillo, J. C. and Filella, M.: Temporal evolution of organic carbon concentrations in Swiss lakes: trends of allochthonous and autochthonous organic carbon, Sci Total Environ, 520, 13-22, 10.1016/j.scitotenv.2015.02.085, 2015.

- Ruff, M., Fahrni, S., Gäggeler, H. W., Hajdas, I., Suter, M., Synal, H.-A., Szidat, S., and Wacker, L.: On-line radiocarbon measurements of small samples using elemental analyzer and MICADAS gas ion source, Radiocarbon, 52, 1645-1656, 2010. Schmid, S. M., Fügenschuh, B., Kissling, E., and Schuster, R.: Tectonic map and overall architecture of the Alpine orogen, 560 Eclogae Geologicae Helvetiae, 97, 93-117, 2004.
- Schwab, M. S., Gies, H., Freymond, C. V., Lupker, M., Haghipour, N., and Eglinton, T. I.: Environmental and hydrologic controls on sediment and organic carbon export from a subalpine catchment: insights from a time series, Biogeosciences, 19, 5591-5616, 10.5194/bg-19-5591-2022, 2022.
- Silva, T. A., Girardclos, S., Stutenbecker, L., Bakker, M., Costa, A., Schlunegger, F., Lane, S. N., Molnar, P., Loizeau, J.-L., and Fielding, C.: The sediment budget and dynamics of a delta-canyon-lobe system over the Anthropocene timescale: The Rhone River delta, Lake Geneva (Switzerland/France), Sedimentology, 66, 838-858, 10.1111/sed.12519, 2019.
 - Sobek, S., Durisch-Kaiser, E., Zurbrügg, R., Wongfun, N., Wessels, M., Pasche, N., and Wehrli, B.: Organic carbon burial efficiency in lake sediments controlled by oxygen exposure time and sediment source, Limnology and Oceanography, 54, 2243-2254, 2009.
- 570 Steinsberger, T., Wüest, A., and Müller, B.: Net Ecosystem Production of Lakes Estimated From Hypolimnetic Organic Carbon Sinks, Water Resources Research, 57, 10.1029/2020wr029473, 2021.
 - Stenström, K. E., Skog, G., Georgiadou, E., Genberg, J., and Johansson, A.: A guide to radiocarbon units and calculations, Lund University, Department of Physics internal report, 1-17, 2011.
- Stutenbecker, L., Delunel, R., Schlunegger, F., Silva, T. A., Šegvić, B., Girardclos, S., Bakker, M., Costa, A., Lane, S. N., and Loizeau, J.-L.: Reduced sediment supply in a fast eroding landscape? A multi-proxy sediment budget of the upper Rhône
 - basin, Central Alps, Sedimentary geology, 375, 105-119, 2018.

 Synal, H.-A., Stocker, M., and Suter, M.: MICADAS: a new compact radiocarbon AMS system, Nuclear Instruments and Methods in Physics Research Section B: Beam Interactions with Materials and Atoms. 259, 7-13, 2007.
 - Tranvik, L., Cole, J. J., and Prairie, Y. T.: The study of carbon in inland waters-from isolated ecosystems to players in the global carbon cycle, Limnology and Oceanography letters, 3, 41-48, 2018.
 - Trumbore, S.: Radiocarbon and soil carbon dynamics, Annual Review of Earth and Planetary Sciences, 37, 47-66, 2009.

580

- White, M. E., Mittelbach, B. V. A., Escoffier, N., Rhyner, T. M. Y., Haghipour, N., Janssen, D. J., Perga, M. E., Dubois, N., and Eglinton, T. I.: Seasonally Dynamic Dissolved Carbon Cycling in a Large Hard Water Lake, Journal of Geophysical Research: Biogeosciences, 130, 10.1029/2024jg008645, 2025.
- Wüest, A., Bouffard, D., Guillard, J., Ibelings, B. W., Lavanchy, S., Perga, M. E., and Pasche, N.: LéXPLORE: A floating laboratory on Lake Geneva offering unique lake research opportunities, Wiley Interdisciplinary Reviews: Water, 8, e1544, 2021.